Device

Article

Prolonged monitoring and risk management of hyperuricemia using interference-resistant wearable bioelectronics

Graphical abstract

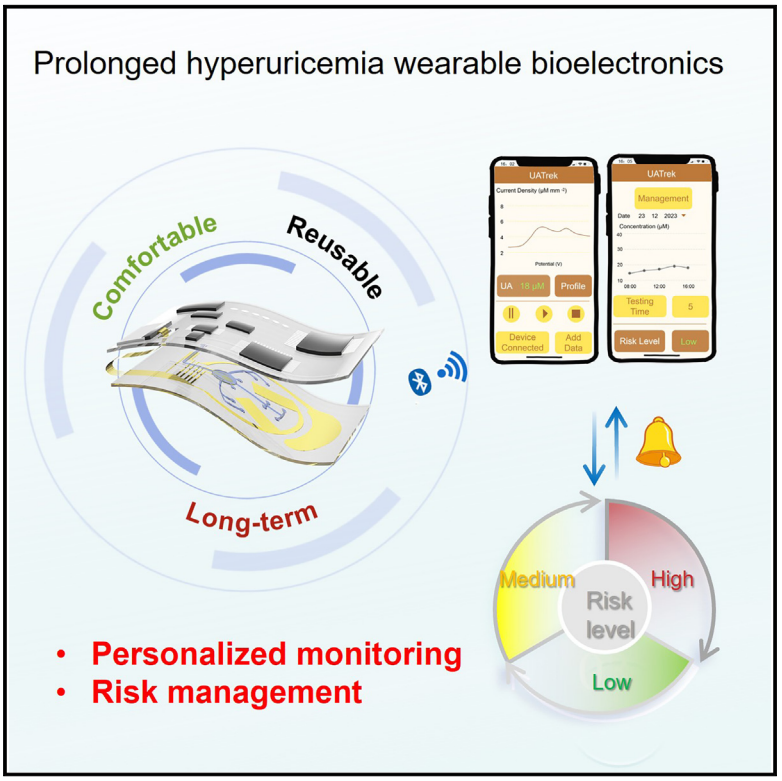

Authors

Yue Hu, Yawen Yang, Hongwei Chu, ..., Yingchun Li, Zhengchun Peng, Xinge Yu

Correspondence

xingeyu@cityu.edu.hk

In brief

Hu et al. developed a flexible device for long-term sensing of hyperuricemia. The employed metal- and polymer-based functionalized electrodes resist by-product deposition and are used to construct a ratiometric sensing mode, enabling accurate uric acid detection over a 15-day period with a deviation of less than 5%.

Highlights

- A wearable platform is developed for prolonged monitoring hyperuricemia
- Bioelectrodes with anti-interference and reusable characteristics
- Wireless telemedicine sensing platform with rapid sample-to-answer turnaround
- Device evaluation in 15-day sweat uric acid tracking of individuals

Develop
Prototype with demonstrated applications in relevant environment

Hu et al., 2025, Device *3*, 100753
July 18, 2025
https://doi.org/10.1016/j.device.2025.100753

CellPress

Please cite this article in press as: Hu et al., Prolonged monitoring and risk management of hyperuricemia using interference-resistant wearable bioelectronics, Device (2025), https://doi.org/10.1016/j.device.2025.100753

Device

CellPress

Article

Prolonged monitoring and risk management of hyperuricemia using interference-resistant wearable bioelectronics

Yue Hu,[1,2,8] Yawen Yang,[1,8] Hongwei Chu,[1,3,8] Rui Shi,[4,8] Jiyu Li,[1] Guoqiang Xu,[1] Xingcan Huang,[1] Binbin Zhang,[1,5] Chun Ki Yiu,[1,5] Guangyao Zhao,[1] Pengcheng Wu,[1] Jian Li,[1,5] Yuan Guo,[1] Qiang Zhang,[1,6] Mengge Wu,[1] Jingkun Zhou,[1,5] Yingchun Li,[3] Zhengchun Peng,[2] and Xinge Yu[1,5,6,7,9,*]

[1]Department of Biomedical Engineering, City University of Hong Kong, Hong Kong, China
[2]State Key Laboratory of Radio Frequency Heterogeneous Integration, College of Physics and Optoelectronic Engineering, Shenzhen University, Shenzhen, China
[3]College of Science, Harbin Institute of Technology, Shenzhen, China
[4]College of Professional and Continuing Education, The Hong Kong Polytechnic University, Hong Kong, China
[5]Hong Kong Centre for Cerebro-cardiovascular Healthy Engineering, Hong Kong, China
[6]Institute of Digital Medicine, City University of Hong Kong, Hong Kong, China
[7]Hong Kong Institute for Clean Energy (HKICE), City University of Hong Kong, Hong Kong, China
[8]These authors contributed equally
[9]Lead contact
*Correspondence: xingeyu@cityu.edu.hk
https://doi.org/10.1016/j.device.2025.100753

THE BIGGER PICTURE Non-invasive wearable biochemical monitoring systems are critically needed for the effective management of chronic metabolic disorders such as hyperuricemia (HUA), hyperglycemia, and hyperlipidemia. Uric acid (UA) quantification holds diagnostic value given that elevated serum levels are strongly associated with HUA and are pathologically linked to gout, cardiorenal syndromes, and metabolic dysregulation. Nevertheless, existing wearable platforms encounter persistent technical barriers, particularly regarding sustained signal accuracy, which is compromised by electrode contamination and biochemical interferents during prolonged operation. In this study, we present a UA monitoring system for tracking UA levels in sweat, as affected by diet and metabolism, which can be used to analyze the individual risk of HUA throughout the day. Based on its long-lasting and reusable properties, the system provides stable signals over a 15-day duration for users.

SUMMARY

We report a prolonged wearable biosensing system for monitoring hyperuricemia (HUA), a prevalent metabolic disorder resulting from abnormal purine metabolism, from sweat, with reliable and stable behaviors for up to 15 days. This reusable wearable system integrates an interference-resistant HUA biosensor, a microfluidic module for autonomous sweat collection, a conformable device-skin adhesive interface with adjustable adhesion strength, and a flexible circuit board for data acquisition and transmission. A customized mobile application provides real-time HUA levels and associated risks, facilitating timely self-regulation and long-term dietary and health management. The HUA sensing signal of sweat was compared and calibrated with clinical standard by serum tests for 80 volunteers, where the results exhibited great correlation and thus can be used as assessing criteria. On-body tracking validation further highlighted the great potential of our wearable bioelectronics for the development of individualized diagnostic protocols.

INTRODUCTION

Wearable sensors using sweat as the sample matrix have applications in personalized health and disease diagnostics as a noninvasive device outside of clinical settings.[1–6] Various sweat-sensing patches have been developed that provide outputs of bio-signals for monitoring multiple metrics.[7–13] However, these technologies are typically limited to short-term use. The reason is that the

Please cite this article in press as: Hu et al., Prolonged monitoring and risk management of hyperuricemia using interference-resistant wearable bioelectronics, Device (2025), https://doi.org/10.1016/j.device.2025.100753

state-of-the-art sweat sensors are based on biosensing electrodes, which have inherent limitations for long-term use and environmental interference resistance.[14–17] Frequent replacement of sweat-sensing patches is expensive and, moreover, they might present differences in sensing performance from batch to batch that would likely cause errors in the detection of trace-level substances in sweat.[18,19]

Researchers are focused on the monitoring of such chronic metabolic diseases involving amino acids, small molecules, and on-body drug metabolism monitoring. These wearable sweat sensors were developed for personalized tracking of dietary intakes, nutrition status, and metabolic syndrome risks.[16,19–21] One of the typical chronic diseases needed for long-term monitoring is hyperuricemia (HUA), which is a metabolic disease caused by abnormal purine metabolism.[22–25] To date, HUA affects over 1 billion people globally, with increasing incidence rates among younger individuals (2023 data).[26] Relevant studies also indicate that patients with HUA face heightened risks of developing hypertension, diabetes, cardiovascular diseases, and cerebrovascular diseases as well as kidney disease and uremia (Figure S1).[27–30] Many patients remain unaware of their HUA status until they experience sudden pain and swelling, such as during a gout attack; in fact, most HUA patients are asymptomatic, with only 20% developing gout within 5 years, often leading to treatment delays.

Traditional blood tests for HUA are insufficient for long-term monitoring because uric acid (UA) levels fluctuate due to lifestyle and dietary habits throughout the day and night.[31,32] Continuous tracking of UA levels and their daily variations are critical. Serum UA monitoring is the clinical standard method; however, the invasive way increases the risk of infection and reduces patient compliance.[33] *In situ* sweat analysis of UA using wearable sensors offers a non-invasive alternative to traditional serum testing.[34–37] However, current wearable sweat-sensing technologies face significant challenges, including the development of long-term reusable and interference-resistant sensors, a durable device-skin interface, and an efficient microfluidic sweat collection system.[38,39]

Here, we present a wearable biosensing platform for prolonged UA monitoring, facilitating effective health management and timely intervention. The platform features a long-term reusable sensing patch that autonomously collects sweat samples and accurately evaluates UA levels in real time through on-site signal processing and wireless communication (Figure 1A). The sensors are designed to prevent the accumulation of UA oxidation by-products while providing a built-in reference signal for ratiometric sensing, making them resilient to environmental disturbances and yielding accurate, stable readings. To ensure long-term wearability and strong adhesion without irritation, the device-skin interface incorporates a hydrogel that combines biocompatibility and temperature-responsive adhesion. Additionally, iontophoresis-based sweat induction technology, hydrophilic microfluidic channels with multiple wrap-around inlets, and a specialized circuit design are employed for efficient sample collection and monitoring. Moreover, we investigated how age and lifestyle factors affect UA levels and their variations. The UA monitor was utilized to track sweat UA levels in healthy individuals and patients with HUA over a consecutive 15-day period.

RESULTS AND DISCUSSION

Design of the UA monitor

The UA monitor is built on a flexible substrate with vertically stacked subcomponents (Figures 1B and S2), minimizing skin contact. Key components include a flexible printed circuit board (FPCB) (Figure 1C) and a microfluidic sweat sensor patch (Figure 1D). All components are reusable, forming a lightweight device that weighs just 2.73 g and adheres closely to the skin, as illustrated in Figures 1E and 1F. The device measures 4.4 cm in length, 3.3 cm in width, and 4 mm in thickness.

The core component, the sweat-sensing patch, consists of an adhesive layer, iontophoresis gels, a hydrophilic microfluidic channel, and a photolithographic electrode (Figure S3). The patch enables long-term sweat collection and accurate UA monitoring. The UA monitor uses a temperature-responsive adhesive hydrogel for soft, conformal contact that accommodates mechanical deformations and allows for easy application and removal without discomfort. The iontophoresis gels and hydrophilic microfluidic channels work synergistically to facilitate perspiration and sample collection. The photolithographic electrode includes a UA sensing module in an elliptical sweat storage region, an iontophoresis module surrounded by microfluidic inlets, and an admittance analysis model at the outlet (Figure S4). UA data acquisition is performed via the FPCB with Bluetooth communication. The systems-level block and circuit diagrams are presented in Figures 1G and S5. A custom mobile application was designed for the analysis, display, and storage of dynamic UA data (Video S1).

Design and evaluation of sweat sensors for prolonged UA analysis and calibration

We developed a UA sensor that measures up to 150 times without cleaning or electrochemical procedures. It features a metal/polymer-based functionalized electrode design and operates in a ratiometric sensing mode to resist interference (Figures S6–S8; Note S1).[40,41] Au nanoparticles (nano Au) enhance the surface area and catalytic activity (Figure S9). A polythionine (pTh) film is electropolymerized on the nano Au substrate, preventing allantoin adsorption through charge repulsion, thus extending reusability (Figure 2A). pTh also generates stable electrical signals, providing a built-in calibration for the ratiometric mode. Sensor responses can be adjusted for factors like pH, temperature, ion concentration, and electrode degradation (Figure S10). Distinct differential pulse voltammetry (DPV) peaks at −0.05 and 0.25 V correspond to the oxidation reactions of pTh and UA, respectively, with the UA concentration significantly enhancing its oxidation peak while leaving the pTh peak stable. After optimization based on cyclic voltammetry (CV) curves and DPV amplitudes (Figures S11–S13; Note S2), we established a standard curve for physiological sweat sample ranges (10–60 μM),[42,43] achieving a sensitivity of 1.93 μA μM^{-1} cm^{-2} and a detection limit of 1.25 μM (Figures 2B, 2C, and S14).

The performance of the fabricated electrodes was evaluated for resistance to by-product deposition and interference from various disturbances. Unlike the gradual decline in response signals observed on the nano Au electrode with repeated tests of the same UA sample (Figure 2D), the fabricated sensors maintained consistent performance (Figure 2E), attributed to the

Please cite this article in press as: Hu et al., Prolonged monitoring and risk management of hyperuricemia using interference-resistant wearable bioelectronics, Device (2025), https://doi.org/10.1016/j.device.2025.100753

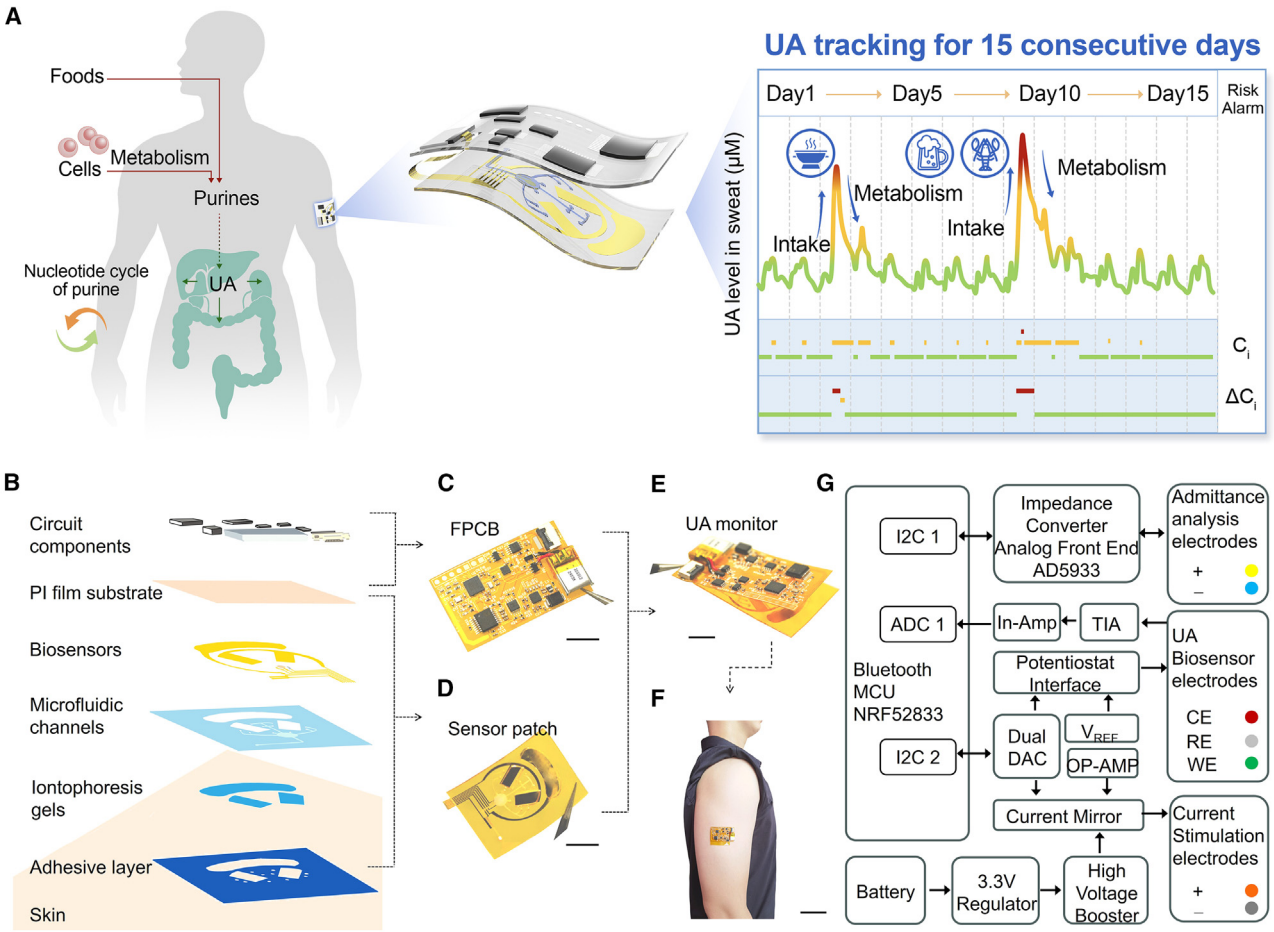

Figure 1. Overview of the wearable bioelectronics for HUA monitoring and management

(A) Schematic of the wearable UA monitor for non-invasive, prolonged, and reusable UA tracking. C_i indicates real-time UA values, and ΔC_i shows concentration fluctuations (μM). Risk levels are represented by green (low), yellow (medium), and red (high) lines.

(B) Magnified view of the wearable UA monitor, showing vertically stacked components.

(C–E) Photographs of an FPCB (C), a UA sensor patch (D), and the complete UA monitor (E). Scale bar, 1 cm.

(F) On-body photo of the fully integrated UA monitor. Scale bar, 3 cm.

(G) Block diagram of the electronic system.

CE, counter electrode; In-Amp, instrumentation amplifier; RE, reference electrode; TIA, *trans*-impedance amplifier; WE, working electrode.

adsorption resistance of pTh. Although the built-in reference signals (J_{pTh}) and UA oxidation response signals (J_{UA}) decreased with increasing DPV test cycles due to diminished electrode performance, this issue can be mitigated by employing a ratio evaluation mode (J_{UA}/J_{pTh}), which improved accuracy over multiple cycles. The constructed electrode successfully sustained 150 consecutive tests, with J_{UA} and J_{pTh} remaining above 70% of their original levels, while the ratio signal of J_{UA}/J_{pTh} consistently exceeded 95%. Subsequently, the repeatability of the UA sensors was evaluated by alternating tests at low (10 μM) and high (40 μM) concentrations. As shown in Figure 2F, the output results at low concentrations were unaffected by high concentration measurements, confirming the reusability necessary for continuous long-term monitoring.

We investigated the advantages of the ratiometric sensing strategy in mitigating external interference. Figures 2G–2I and S15 and Note S3 showed sensor outputs in response to changes in pH, temperature, and ionic strength, demonstrating that our UA sensors are stable against environmental factors. We also investigated the impact of extreme conditions, such as electrode breakage from prolonged sweat immersion or external forces, on output stability (Figures 2J, 2K, and S16). The relative standard deviation of the ratiometric means (I_{UA}/I_{pTh}) was reduced by at least 50 times compared to that of UA signal alone (I_{UA}), even with varying degrees of electrode loss. We studied the accuracy and reliability of the sensing electrodes for analyzing artificial sweat samples via the standard addition method (Figure S17), achieving a high correlation coefficient of 0.985. Long-term reliability tests showed that in single-signal mode (J_{UA}), accuracy was maintained for only 20 days, with J_{UA} decayed to 90% of their initial signals after this period (Figures 2L and S18). In contrast, J_{UA}/J_{pTh} responses remained stable for 60 days. The

Please cite this article in press as: Hu et al., Prolonged monitoring and risk management of hyperuricemia using interference-resistant wearable bioelectronics, Device (2025), https://doi.org/10.1016/j.device.2025.100753

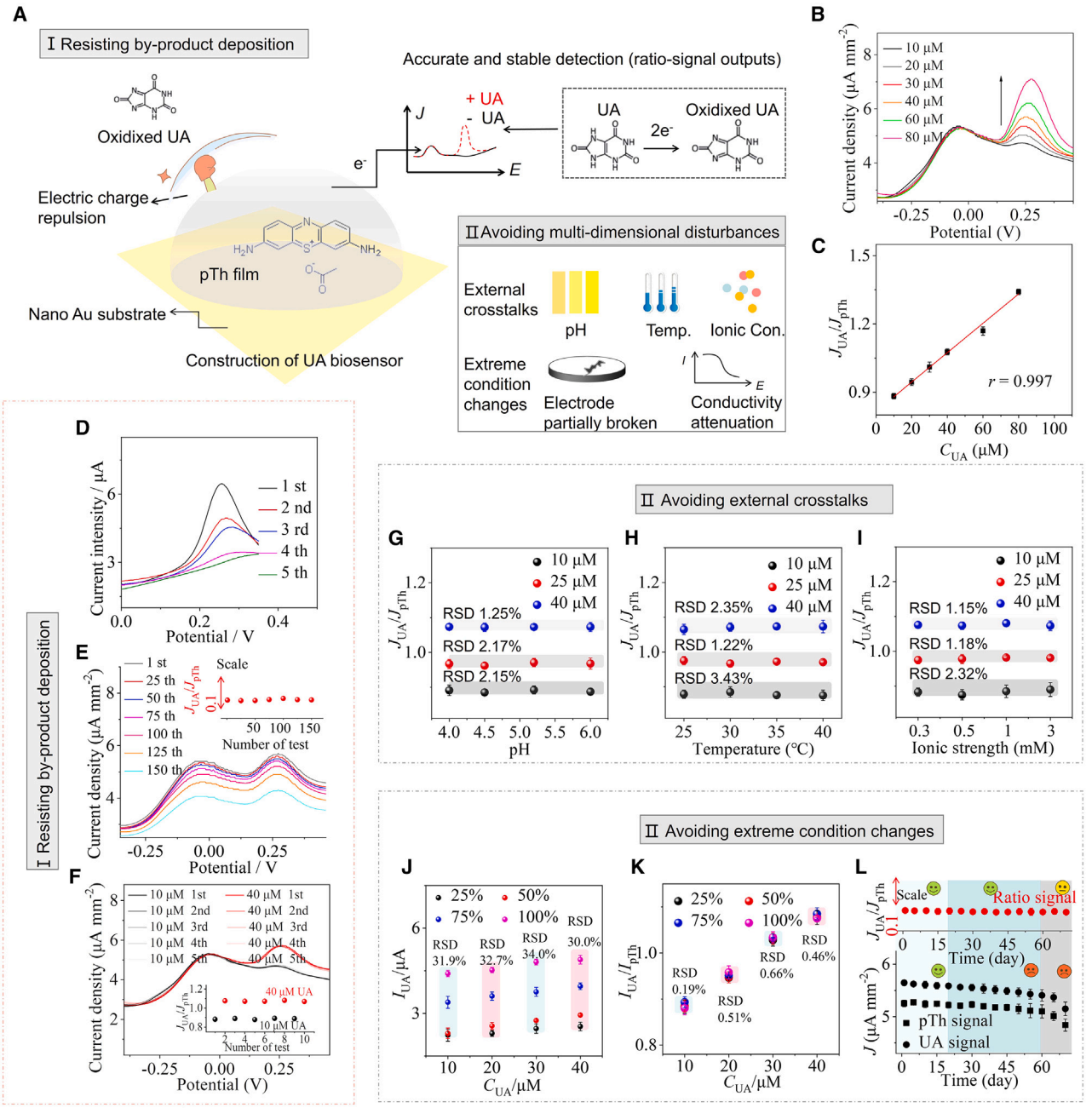

Figure 2. Schematics and characterization of UA sensors

(A) Fabrication process and sensing principle of our ratiometric sensor for UA detection using pTh to resist by-product deposition and external/internal interference.

(B) DPV responses of a UA ratiometric sensor for UA quantification.

(C) Calibration plot with linear fit.

(D) Repetitive DPV responses of an unmodified nano Au electrode to a 40-μM UA sample over three independent trials without cleaning.

(E) Continuous DPV responses from the ratiometric sensor to a 40-μM UA sample, with an inset showing calculated ratio signals vs. test number.

(F) Alternating DPV responses to low (10 μM) and high (40 μM) UA concentrations, where odd tests correspond to low concentration and even tests to high concentration.

(G–I) Sensor response dependence on pH (G), temperature (H), and ionic strength (I).

(J and K) Dot plots of UA current signals (I_{UA}) (J) and the ratio current signal of UA and pTh (I_{UA}/I_{pTh}) (K), with varying sensor working areas for different UA concentrations.

(L) Long-term reliability of sensors after activation, showing current densities of UA and pTh and their ratio over storage time. All error bars indicate standard deviation from three parallel tests.

Please cite this article in press as: Hu et al., Prolonged monitoring and risk management of hyperuricemia using interference-resistant wearable bioelectronics, Device (2025), https://doi.org/10.1016/j.device.2025.100753

reproducibility, sensing stability against deformation tests, and selectivity of our sensors were also evaluated, as shown in Figures S19–S21 and Table S1.

Wearable system design for long-term and autonomous sweat induction and sampling

To enable long-term perspiration sampling for monitoring UA changes, the wearable patch was designed with multiple layers: a temperature-responsive hydrogel (PCPG hydrogel) serving as the patch-skin interface for on-demand adhesion and removal, an iontophoresis module for adjustable sweat induction, a hydrophilic microfluidic module for efficient sweat transport to the sensing area; a ratiometric sensing module for accurate UA monitoring, and an electrode admittance analysis model at the microfluidic outlet to quantify sweat (Figure 3A). As illustrated in Figures 3B and S22A, when the high concentration UA sample (40 μM) was pumped into our microfluidic system filled with low-concentration sample (10 μM), the real-time current density of the oxidation peak was continuously updated with a 30-s DPV scan every minute, stabilizing within 4 min (Figure S22A). The response signal gradually returned to its initial level when the UA input switched from high to low concentration (Figure S22B), demonstrating the system's ability to update samples and for high temporal resolution.

The iontophoresis module for sustainable sweat extraction comprised an Au-based anode and cathode with hydrogels containing carbachol and NaCl. Carbachol was chosen for its ability to induce repeatable and long-lasting perspiration from sweat glands. Optimization focused on carbachol concentration and electrode current intensity, as these significantly impact the perspiration rate of sedentary individuals (Figures S23A and S23B). The optimal conditions identified were 1% carbachol and a 500-μA current (Figures S23C and S24). To accommodate variability in sweating rates among individuals, we recorded DPV response curves of our sensing patch at physiological sweat rates from 0.5 to 3 μL min^{-1}. As illustrated in Figures 3C and S25, the sensing patch delivered stable readings across different flow rates.

To enhance the functionality of the polydimethylsiloxane (PDMS)-based microfluidic channels for sweat guidance and transportation, we applied a layer of mono-dispersed silica microspheres (SiO_2) to improve hydrophilicity (Figure 3D). SiO_2-treated PDMS maintained the hydrophilicity even after 50 consecutive soaking and drying cycles (Figure S26),[44] resolving issues with sweat collection and preventing collapse of the liquid storage area. Additionally, a layer of semi-scalloped SiO_2 at the channel outlet facilitated excess sweat infusion (Figure S27). We designed an electrode admittance analysis model at the outlet, with Au triggering electrodes that connect when sweat flows through, creating a current path. The conduction mechanism is illustrated by an equivalent circuit model (Figure 3F), with C_d, R_{ct}, and R_s representing double-layer capacitance, charge transfer resistance, and solution resistance, respectively. Experimental results revealed that sweat reaching the electrodes caused the admittance pulse to transition from nS to mS, indicating adequate sweat collection (Figure 3G). Analysis of dynamic and static samples (Figure 3H) confirmed that admittance fluctuations reflect perspiration stability. As illustrated in Figures 3I and S28–S30 and Note S4, with the optimized design (10 inlets, 180° span, and aligned to outlet) and 1.0 μL min^{-1} as the inlet sweat rate, the simulated refreshing time was around 150 s for a sample concentration change of 10–40 μM. During on-body trials, sweat was locally induced and sampled with high temporal resolution, expelling pre-injected red ink through the microchannels outside the sensing area (Figure 3J).

To meet the long-term wearable demands of the sensor patch, we designed a temperature-responsive adhesive hydrogel (PCPG hydrogel) synthesized from chitosan (CS), poly(vinyl alcohol) (PVA), phytic acid (PA), and gelatin (Figure S31). The PCPG hydrogel serves as the device-skin interface, providing reversible and painless adhesion and detachment when triggered by temperature (Figures 3K and S32A; Video S2). At 10°C, the adhesion strength of the hydrogel diminishes significantly, while it increases at 37°C after several minutes (Figure 3L). Results from Figures 3M and S33–S35, Note S5, and Table S2 confirm that the PCPG hydrogel meets long-term wearability requirements.

Evaluation of the device for dynamic sweat UA monitoring

Sweat-induction methods are categorized into active perspiration during exercise and passive perspiration via iontophoresis at rest (Figure 4A). For daily UA monitoring, iontophoresis is preferable for prolonged dynamic sampling. Significant water loss from intense exercise can create inconsistencies in UA levels between sweat and serum, leading to distorted results. As illustrated in Figure 4B, sweat UA levels decreased during badminton exercise, likely due to excessive sweating. In contrast, prolonged exercise caused a temporary rise in serum UA levels. However, stable sweat UA data were obtained from two subjects using an iontophoresis-integrated patch at rest, which aligned with serum levels (Figure 4C). These results confirmed that passive perspiration via iontophoresis is more effective for sweat UA detection than exercise-induced perspiration.

To evaluate the feasibility of the UA monitor in practical applications, a controlled purine-diet study was conducted with two groups of healthy individuals: normal group (n = 3) and purine-rich group (n = 3). UA concentrations in sweat and serum were tracked over three consecutive fasting mornings. Both serum and sweat UA levels increased in the purine-rich group, while the normal group showed little fluctuation during the tests without additional purine intake (Figures 4D and 4E), consistent with previously reported results.[16,43] Furthermore, the UA monitor could screen out abnormal individuals (subjects with HUA, n = 3, and gout patients, n = 2) among healthy individuals (n = 5), where there is little difference in UA levels between gout patients and subjects with HUA because there is no necessary correlation between high UA levels and gout attacks[38] (Figure 4F). Our pilot study demonstrated that the placement of sensor patches on different body parts had a minimal effect on readings (Figure S36). To demonstrate the feasibility of the wearable system for dynamic UA monitoring, we recorded changes in sweat and serum UA levels from 11 a.m. to 9 p.m. in four healthy subjects (Figure S37), where trends in both body fluids were consistent. We established a correlation between sweat and serum UA levels based on data from 80 independent human samples, yielding a correlation coefficient of 0.941 (Figure 4G).

Please cite this article in press as: Hu et al., Prolonged monitoring and risk management of hyperuricemia using interference-resistant wearable bioelectronics, Device (2025), https://doi.org/10.1016/j.device.2025.100753

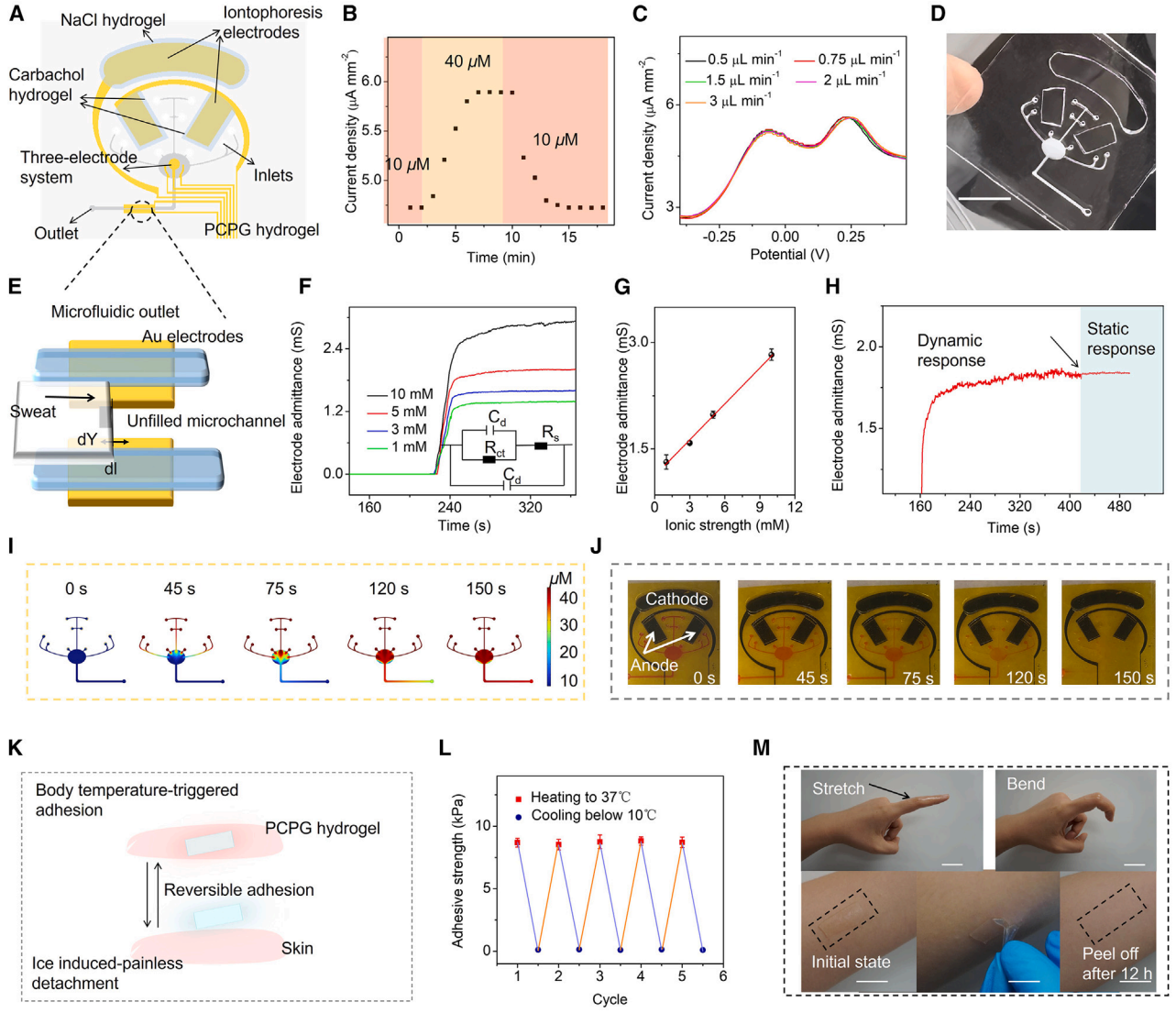

Figure 3. Design of the wearable system for long-term and autonomous sweat induction and sampling

(A) Illustration of a wearable sensor patch for long-term UA sensing.

(B) Current density vs. time (1–18 min) plots, with a flow rate of 1.5 μL min^{-1} and DPV scans every minute (range: 0.05–0.4 V).

(C) DPV voltammograms from the sensor for 40 μM UA at various flow rates (0.5–3 μL min^{-1}).

(D) Optical photographs of the microfluidic patch post-hydrophilic modification. Scale bar, 1 cm.

(E) Schematic of the electrode admittance analysis model at the microfluidic outlet.

(F) Electrode admittance of PBS with different concentrations at an injection rate of 1 μL min^{-1}. Inset shows equivalent circuit model.

(G) Calibration curve of electrode admittance vs. electrolyte concentrations.

(H) Investigation of electrode admittance with and without electrolyte flow at the microchannel outlet, indicating the flow-stationary transition point.

(I and J) Numerically simulated UA concentration distributions (I) and on-body testing of the flexible microfluidic reservoir for carbachol-based sweat induction at rest (J), using 1% carbachol and 500 μA current, with red ink for visualization.

(K) Illustration of temperature-triggered adhesion and ice-induced painless detachment of the PCPG hydrogel.

(L) Adhesive strength of PCPG hydrogel to pigskin at 37°C and 10°C.

(M) Photographs of PCPG hydrogel on human skin and allergy test results. Scale bar, 2 cm.

Personalized management of HUA using the UA monitor

Continuous monitoring of UA levels enables early detection of asymptomatic UA metabolic risk, facilitating personalized risk alerts, dietary interventions, and UA-lowering therapy (Figures 5A and S38). Specifically, the UA monitor focuses on real-time UA value ($C_{1\text{-}0}$, $C_{1\text{-}1}$, $C_{1\text{-}n}$, …, $C_{2\text{-}0}$, …) risk as well as the risk of UA changes ($\Delta C_{1\text{-}1}$, $\Delta C_{1\text{-}n}$, …, $\Delta C_{2\text{-}n}$, …) by recording UA levels throughout the day. Based on the established correlation between UA values in serum and sweat, the risk levels for real-time UA values are defined as follows: C_i <25 μM (equivalent to serum UA <420 μM) is considered low risk; 25 μM ≤ C_i <35 μM (equivalent to 420 μM ≤ serum UA <540 μM) is medium

Please cite this article in press as: Hu et al., Prolonged monitoring and risk management of hyperuricemia using interference-resistant wearable bioelectronics, Device (2025), https://doi.org/10.1016/j.device.2025.100753

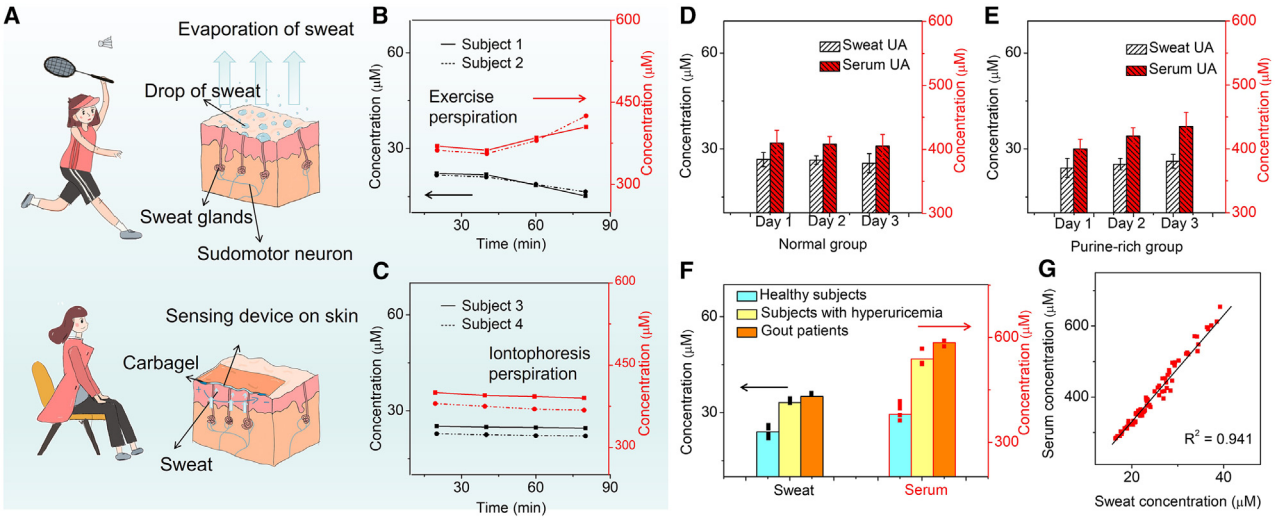

Figure 4. Evaluation of the wearable system for dynamic sweat UA monitoring

(A) Schematic of sweat formation through exercise and iontophoresis.

(B and C) UA levels in sweat and serum during exercise (B) and iontophoresis (C) perspiration.

(D and E) Sweat and serum UA levels under regular (D) and purine-rich diets (E) over 3 days, with error bars representing standard deviation at 10 a.m. ($n = 3$ for each diet group).

(F) Comparison of UA levels in sweat and serum among gout patients, HUA subjects, and healthy individuals, with dots representing UA values ($n = 2$ for gout, $n = 3$ for HUA, $n = 5$ for healthy patients).

(G) Correlation between serum and sweat UA concentrations from 80 biologically independent samples.

risk, C(M); and $C_i \geq 35$ μM (equivalent to serum UA ≥ 540 μM) indicates high risk, C(H). For evaluating fluctuations in UA values, $\Delta C_i < 5$ μM (equivalent to fluctuations of serum UA <60 μM) is low risk; 5 μM $\leq \Delta C_i < 10$ μM (equivalent to 60 μM $\leq$ fluctuations of serum UA <120 μM) is medium risk, ΔC(M); and $\Delta C_i \geq 10$ μM corresponds to fluctuations in serum UA ≥ 120 μM, classified as high risk, ΔC(H). Elevated circulating UA levels and significant fluctuations are concerning,[45] as they directly contribute to HUA and are strongly associated with diabetes, coronary heart disease, cerebrovascular disease, hypertension, and chronic kidney disease.

Collecting personal information from 50 randomized patients with HUA revealed common traits, including a higher prevalence of males, a predominance of middle-aged and younger adults, and a high body mass index (BMI) (Figures 5B and 5C). This indicates that individual UA levels are influenced by a variety of factors, such as lifestyle, dietary habits, metabolism, and genetics. We carried out a pilot study using simple control variables to investigate the correlation between UA levels and age throughout the day, involving three groups of subjects: youth (25 $\leq$ age <40), middle-aged (40 $\leq$ age <60), and elderly (age $\geq$60). Participants in the elderly group had lower UA levels and slower fluctuations throughout the day compared to the middle-aged and younger groups, likely due to their dietary habits and reduced food intake (Figures 5D and S39). Additionally, UA levels tended to be slightly higher in males than females within the same age group, consistent with previous reports. We also examined the effects of long-term preferential intake of meat, sugary beverages, and alcohol on circulating UA (Figure S40), which can lead to HUA and even gout attacks. In all subjects, UA levels varied with daily routines and meal intake. As shown in Figures 5E–5G, high consumption of meat and beer led to a significant increase in UA levels over time, attributable to high purine intake and impaired UA metabolism.[46–48]

To evaluate the potential applications of the UA monitor for long-term monitoring of UA levels, risk warnings, and dietary and medication guidance, we initiated a 15-day study measuring UA levels in sweat from four healthy individuals and two patients with HUA (Figure 5F). Results from healthy subject 1 indicated that a high-purine diet significantly affected circulating UA levels over a short period. On the third day, the intake of high-purine hot pot resulted in C(M) and ΔC(H), while the intake of both seafood and beer on the ninth day caused both C(H) and ΔC(H). Notably, excessive purine intake likely causes increased UA levels the following day, and possibly the third day, due to the time required for the body to metabolize and excrete the excess UA.[49] Meanwhile, UA levels in healthy subjects 2, 3, and 4 (Figure S41) exhibited consistent and flatter fluctuations over the 15-day period when following normal or low-purine diets. Furthermore, the UA monitor was employed to track sweat UA fluctuations over the same period in two HUA patients, one on initial drug therapy and the other on long-term medication (Figure S42). The above results validated the potential of the UA monitor for personalized dosage adjustments in UA-lowering therapy.

Conclusions

In conclusion, we have developed a wearable UA sensing system capable of prolonged tracking of UA in sweat, featuring resistance to interference. This technology can analyze individual risks of HUA. By correlating on-body sweat test results from a large number of experimental samples with serum measurements, we have established assessment criteria for the UA

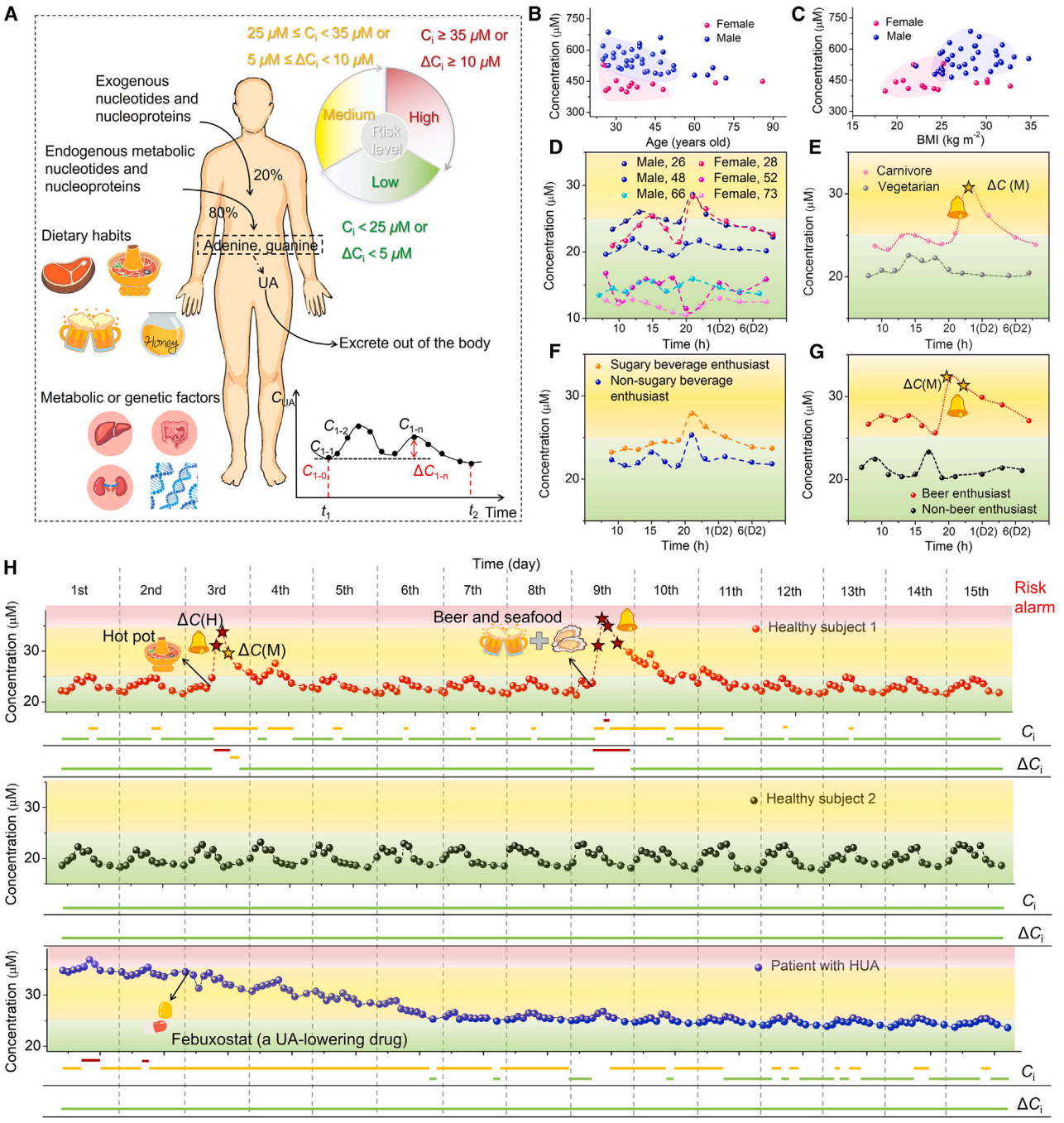

Figure 5. On-body evaluation of the wearable patch toward personalized and non-invasive HUA management

(A) Association between metabolic nucleotides, nucleoproteins, and HUA risk levels throughout the day.

(B and C) Scatterplots showing the relationship between age (B) and BMI (C), with serum UA concentrations from 50 random HUA patients, highlighting common age and BMI ranges.

(D) Recorded UA fluctuations in healthy individuals of different ages and genders on a random day.

(E) Comparison of sweat UA fluctuations between a 30-year-old vegetarian male and a 29-year-old male meat lover with similar BMI.

(F) Sweat UA levels in a 27-year-old male sugary beverage enthusiast vs. a 31-year-old male non-sugary beverage enthusiast.

(G) Sweat UA levels in a 50-year-old male beer enthusiast vs. a 51-year-old male who did not drink beer.

(H) Sweat UA levels recorded over 15 days in 3 individuals: Healthy subject 1 (male, 27 years old) with high-purine intake on the third and ninth days; healthy subject 2 (female, 25 years old) with no high-purine diet; and a 32-year-old male HUA patient taking febuxostat from the third day. Δ*C*(M) and Δ*C*(H) indicate increases in UA concentration to medium and high risk levels, respectively.

Please cite this article in press as: Hu et al., Prolonged monitoring and risk management of hyperuricemia using interference-resistant wearable bioelectronics, Device (2025), https://doi.org/10.1016/j.device.2025.100753

monitor, yielding high correlation coefficients in the pilot study. The long-lasting and reusable properties of the UA monitor have been validated, demonstrating reliable and stable signal collection over a 15-day period with users. We anticipate that this technology will provide new insights into the design of non-invasive, long-term monitoring systems for various chronic disease-related biomarkers, facilitating a wide range of personalized preventive, diagnostic, and therapeutic applications. We envision that the UA monitor could serve as a reference for the development of low-cost long-term biosensing devices, expanding the application of wearable technology in chronic disease healthcare monitoring. Looking ahead, we see exciting opportunities to expand our technology beyond UA to monitor various chronic disease biomarkers, creating comprehensive wearable health systems for real-time insights. Additionally, we aim to integrate the UA sensing system with existing mobile health applications, providing users immediate feedback to encourage proactive health management and lifestyle changes.

METHODS

Materials and reagents

UA, thionine (Thi), CS, alanine, ascorbic acid, creatine, glucose, lactate, serine, and Au acid chloride trihydrate ($HAuCl_4 \cdot 3H_2O$) were purchased from Alfa Aesar (Shanghai, China). Arginine, aspartic acid, citruline, creatinine, glutamic acid, glycine, histidine, inositol, nicotinic acid, pantothenic acid, riboflavin, thiamin, threonine, tyrosine, and valine were purchased from Thermo Fisher Scientific (Waltham, MA). Agarose, carbachol, gelatin, PA, and PVA were supplied by Adamas Reagent Company (Shanghai, China). Sodium dodecylbenzenesulfonate (SDBS), glycerol, polymethyl methacrylate (PMMA), mono-dispersed silica microspheres (SiO_2), $K_3[Fe(CN)_6]$, $K_4[Fe(CN)_6]$, $FeCl_3$, $CaCl_2$, KCl, and NaCl were obtained from Sigma-Aldrich (St. Louis, MO). Photoresist (PR, AZ 4620) and AZ 400K solution were purchased from the AZ Electronic Materials (Suzhou, China). PDMS (Sylgard 184 Kit) was obtained from Dow Corning (Midland, MI).

Fabrication and characterization of the UA sensors

The UA sensors were fabricated on a polyimide (PI) film (75 μm) as a supporting substrate The PI film was cleaned with deionized (DI) water, ethanol, and acetone. A layer of Cr/Au (10 nm/100 nm) was coated using an e-Beam Evaporation System. To obtain the custom pattern, a PR layer was spin-coated on the PI/Cr/Au membrane at 500 rpm for 10 s, 3,000 rpm for 30 s, and baked at 110°C for 5 min. Then, it was exposed to ultraviolet (UV) light for 45 s with the help of custom mask and a URE-2000 mask aligner model to operate photolithography. After treating with UV light, it was developed for 1 min in AZ 400K solution ($V_{developer}$:V_{water} was set as 1:3). Finally, Au and Cr were etched accordingly, followed by acetone to remove the residual PR. For the working electrode, nano Au and Thi were electrochemically prepared on the Au electrode (Figures S43 and S44). The nano Au was electrodeposited in 0.5 M H_2SO_4 with 10 mM $HAuCl_4$ at 0.15 V for 30 s. Thi was polymerized via CV from −0.4 to 0.4 V at 0.1 V s^{-1} for 30 cycles in a 5-mM solution at pH 6.0. The reference electrode was prepared by screen printing Ag/AgCl ink onto an Au film and drying overnight, while the counter electrode remained unmodified. The morphology of the modified electrodes was characterized by an environmental scanning electron microscope (Quanta-250, FEI Corporation, Hillsboro, OR).

All *in vitro* electrochemical characterizations for the UA sensor were conducted on an electrochemical workstation (CHI 660, Shanghai Chenhua, Shanghai, China). The UA sensor's response was recorded using DPV in 0.3× PBS (pH 6.0) and raw sweat with varying UA levels. The DPV parameters included scan range −0.5 to 0.5 V, incremental potential 0.004 V, pulse amplitude 0.05 V, pulse width 0.05 s, pulse period 0.5 s, and sensitivity 1×10^{-5} A V^{-1}. Selectivity was assessed in PBS containing physiological analyte concentrations. The sensor response dependence on pH, temperature, and electrolyte concentration was studied in PBS with varying pH levels (4.5, 5.2, 6.0, 6.5), temperatures (25°C, 30°C, 35°C, 40°C), and ionic concentrations (3, 1, 0.5, 0.3 mM). Electrochemical kinetics of the UA sensor and its preparation process were characterized using CV in probe aqueous solution containing 0.1 M KCl and 5 mM $[Fe(CN)_6]^{3-/4-}$.

Fabrication of hydrogels with thermoresponsive adhesive

PCPG hydrogel was prepared with a facile two-step strategy. First, 1.08 g PVA, 0.12 g gelatin, and 0.15 g CS were mixed well. Second, 3 g glycerol-water binary solvent (1:4) and 6 mL PA aqueous solution were added sequentially while stirring. The suspension was water bath heated at 80°C until it became a clear liquid. The liquid was then poured into the adhesive layer mold and transferred to −20°C for 20 h for internal hydrogen bond formation after cooling to room temperature. As displayed in Figure S2, the prepared PCPG hydrogel (bottom layer) served as the double-sided adhesive layer in contact with the skin, patterned with iontophoresis gel and inlets to allow current flow from the top iontophoresis electrodes. Other thermoresponsive adhesive hydrogels were synthesized in a similar manner, and their components and properties are summarized in Table S2.

Mechanical performances of PCPG hydrogel

Adhesion tests of hydrogels

The adhesive strength of the fabricated hydrogels with different contents ratio was measured by a simple adhesion-tensile test with a tensile testing machine (Chuanbai, WDW-50D). Fresh porcine skin was selected as the typical tissue. The hydrogel was attached to the porcine skin over a bonding area of 25 × 25 mm and preloaded with 20 N for a few seconds. Then, it was pulled with a 100-N loading with a crosshead speed of 2 mm min^{-1} at body temperature (37°C) until separation. The adhesion strength was calculated by dividing the maximum load by the bonding area. The temperature-triggered adhesion behavior of the hydrogels was assessed by testing the adhesive strength of the samples at 37°C and 10°C alternately.

Water retention

The hydrogels were stored under a constant temperature (37°C) and humidity of 60%. Their weight was recorded daily at fixed intervals. The weight ratio was calculated by dividing the recorded weights of the hydrogels at different time points by their initial weights.

Please cite this article in press as: Hu et al., Prolonged monitoring and risk management of hyperuricemia using interference-resistant wearable bioelectronics, Device (2025), https://doi.org/10.1016/j.device.2025.100753

Fabrication and characterization of microfluidic channels

The microfluidic channels were fabricated via photolithography method and PDMS replica molding. A silicon master was created by spin-casting SU-8 2050 (MicroChem, Round Rock, TX) at 1,250 rpm for 30 s, followed by soft-baking at 65°C for 5 min and 95°C for 15 min. The master was then UV exposed (230 mJ/cm^2), post-baked at 65°C for 5 min and 95°C for 10 min, and developed for 10 min, resulting in 100-μm deep channels. An anti-adhesion layer of PMMA was added, cured at 180°C. Next, PDMS mixed with a curing agent in a 10:1 ratio was spin-coated at 200 rpm and cured at 70°C for 4 h, yielding a 400-μm thick inverse replica. The microfluidic layer included ten 1-mm inlets, an elliptical reservoir (5 × 4 mm), and 200-μm-wide microchannels, with a reservoir volume of approximately 1.6 μL. To enhance hydrophilicity, the PDMS was treated with a 1% PVA solution containing 1% SiO_2 and 0.5% SDBS. Finally, the treated PDMS was then sealed to another flat PDMS slab or a biochemical sensing substrate using oxygen plasma treatment for 5 min and baked at 70°C for 15 min, followed by sealing verification with DI water.

The liquid flow behavior in the microchannels was simulated with COMSOL Multiphysics 6.0. Three-dimensional models of various microfluidic designs were created in AutoCAD and imported into COMSOL. Each model was simplified as an incompressible laminar flow and the transport of diluted species module. Mass transport was simulated by numerically solving the Navier-Stokes equations coupled with convection-diffusion equations. The prescribed total flow rate was 1 μL min^{-1}, with non-slip boundary conditions applied to all channel walls. An initial UA concentration value of 10 μM was set, along with a new UA concentration of 40 μM and a diffusion coefficient of 1 × 10^{-9} m^2/s for all cases. Concentration changes over time were tracked to show concentration profiles in Figures S29 and S30.

Fabrication of agonist agent hydrogels

Iontophoresis hydrogels were prepared as follows. For carbachol hydrogel, 0.3 g agarose was added into DI water and heated to 250°C under continuous stirring until it became homogeneous. Once cooled to 55°C, 0.1 g carbachol was added. The cooled mixture was poured into a pre-made anodic hydrogel mold and solidified for 10 h at 4°C. The cathode hydrogel (NaCl hydrogel) was fabricated similarly, except that 0.1 g NaCl was used instead of carbachol.

Signal conditioning, processing, and wireless transmission for the wearable sensor

Sweat induction

The programable constant current source and impedance measurement module was applied to the sweat induction. The current source was built with a current mirror using an operational amplifier (AD8541, Analog Devices, Wilmington, MA) and an N-type MOSFET (BSS138BKVL, Nexperia, Nijmegen, the Netherlands). Due to the skin's high impedance, high voltage from a booster (TPS61391RTER, Texas Instruments, Dallas, TX) was applied to the MOSFET. The constant current was controlled via output channel A of a dual digital-to-analog converter (DAC) (DAC60502, Texas Instruments) with I2C communication. The impedance measurement module utilized an analog front-end chip (AD5933, Analog Devices) to monitor sweat collection. When the electrical impedance reached a defined threshold, indicating sufficient sweat collection, the impedance data were sent to the microcontroller, which then shut down the constant current source.

Sweat sensing

DPV measured UA concentration using a potentiostat interface built with a dual operational amplifier (AD8606, Analog Devices) and a DAC (DAC60502, Texas Instruments). The dual operational amplifier facilitated the three-electrode system and acted as a current-to-voltage converter, while the DAC provided dynamic excitation signals to bias the reference and working electrodes. The microcontroller's integrated analog-to-digital converter captured the analog voltage signals, which were then processed and transmitted to a user device via Bluetooth.

Human subject recruitment

All experiments involving human subjects were approved by the research committee of City University of Hong Kong and conducted in compliance with the guidelines. Participation in the studies was fully voluntary, with all participants providing written informed consent. Subjects aged over 18 years were recruited from the City University of Hong Kong campus, neighboring communities, and the People's Hospital of Nanshan District in Shenzhen, China. All subjects submitted written informed consent before participation in the study.

On-body system validation

For the iontophoresis perspiration group, subjects' arms were cleaned with alcohol swabs before applying sensor patches. If necessary, the device can be packaged for testing. The encapsulation involves mixing Ecoflex elastomer parts A and B in a 1:1 ratio, vacuuming to remove air bubbles, and pouring the mixture over the unit while ensuring the outlet of the microchannel remains clear for sweat discharge (Figure S45). During a 5-min iontophoresis session, the system sent an admittance pulse between Au electrodes every second. If admittance exceeded a threshold, the first DPV scan for UA detection started (Figure 3E). Data were wirelessly sent to the user interface via Bluetooth and converted to concentration levels based on a calibration curve (Figure 2C). The UA test intervals were customizable. For the exercise perspiration group, sweat samples from subjects' foreheads and necks were collected in centrifuge tubes and analyzed every 20 min until exercise ceased (Figure 4A).

Serum UA levels were measured through venous or fingertip blood sampling using a chemical analyzer or fingertip UA tester. In a controlled purine-diet study, six healthy males were recruited: three from a normal group and three from a purine-rich group (Figures 4D and 4E). Fasted UA levels in sweat and serum were recorded for all participants on the first day. The normal group maintained a daily diet, while the purine-rich group had a high-purine diet for 2 days. We also recruited two gout patients, three HUA patients without a gout history, and five healthy subjects (Figure 4F). All patients had not taken urate-lowering medication for at least 1 week before the study.

Integrated system validation for prolonged risk alarms and personalized management

To evaluate the performance of the UA monitor for prolonged monitoring, subjects underwent an initial sweat UA test upon waking. Test intervals were set at 2 h during the day and 4 h at night, adjustable to individual routines. To examine the impact of chronic meat intake, sugary beverage consumption, and alcohol on circulating UA (Figures 5E–5G, S39, and S40), we recruited volunteers of similar age and gender with varying dietary habits. For a 15-day tracking of sweat UA levels (Figures 5H, S41, and S42), internal iontophoresis hydrogels (carbachol and NaCl) were replaced each morning to ensure reliable sweat extraction. During the long-term monitoring, decisions on encapsulation were based on individual behavior. The device can withstand less than 5 min of simulated light rain (Figure S46). To achieve waterproof performance against bathing or prolonged exposure to water, encapsulation is required.

RESOURCE AVAILABILITY

Lead contact

Further information and requests for resources and reagents should be directed to and will be fulfilled by the lead contact, Xinge Yu (xingeyu@cityu.edu.hk).

Materials availability

This study did not generate new unique reagents.

Data and code availability

All data in this study are available within the article and supplemental information. The data and code that support the conclusions of this study are also available from the lead contact upon reasonable request.

ACKNOWLEDGMENTS

This work was supported by the National Natural Science Foundation of China (grant no. 62122002); the City University of Hong Kong (grant nos. 9667221, 9678274, and 9610444), as part of the InnoHK Project 2.2–AI-based 3D ultrasound imaging algorithm at Hong Kong Center for Cerebro-cardiovascular Health Engineering (COCHE); the Research Grants Council of the Hong Kong Special Administrative Region (grant nos. RFS2324-1S03, 11213721, 11215722, and 11211523); and the Shenzhen Science and Technology Innovation Commission (grant no. SGDX20220530111401011).

AUTHOR CONTRIBUTIONS

X.Y. and Y.H. conceived the idea and designed the project. X.Y. supervised the work. Y.H. designed the whole system and conducted the overall experiments. Y.H., H.C., X.H., P.W., and Jian Li contributed to sensor characterization and validation. R.S., Jiyu Li, G.X., B.Z., and Y.G. led the design, customization, and simulation of the microfluidic modules. Y.Y., C.K.Y., and J.Z. designed the circuits. Y.H., H.C., G.Z., Q.Z., M.W., Y.Y., P.W., and R.S. contributed to the design of the human trials and to the system's evaluation in the participants. All authors contributed to data analysis and provided feedback on the paper.

DECLARATION OF INTERESTS

The authors declare no competing interests.

SUPPLEMENTAL INFORMATION

Supplemental information can be found online at https://doi.org/10.1016/j.device.2025.100753.

Received: November 14, 2024
Revised: November 15, 2024
Accepted: February 28, 2025
Published: March 27, 2025

REFERENCES

1. Min, J., Tu, J., Xu, C., Lukas, H., Shin, S., Yang, Y., Solomon, S.A., Mukasa, D., and Gao, W. (2023). Skin-interfaced wearable sweat sensors for precision medicine. Chem. Rev. *123*, 5049–5138. https://doi.org/10.1021/acs.chemrev.2c00823.
2. Kim, J., Campbell, A.S., de Ávila, B.E.F., and Wang, J. (2019). Wearable biosensors for healthcare monitoring. Nat. Biotechnol. *37*, 389–406. https://doi.org/10.1038/s41587-019-0045-y.
3. Lorestani, F., Zhang, X., Abdullah, A.M., Xin, X., Liu, Y., Rahman, M., Biswas, M.A.S., Li, B., Dutta, A., Niu, Z., et al. (2023). A highly sensitive and long-term stable wearable patch for continuous analysis of biomarkers in sweat. Adv. Funct. Mater. *33*, 2306117. https://doi.org/10.1002/adfm.202306117.
4. An, Z., Fu, Q., Lv, J., Zhou, T., Wu, Y., Lu, Y., Liu, G., Shi, Z., Li, X., Zhang, F., and Liu, Q. (2023). Body heat powered wirelessly wearable system for real-time physiological and biochemical monitoring. Adv. Funct. Mater. *33*, 2303361. https://doi.org/10.1002/adfm.202303361.
5. Ye, C., Wang, M., Min, J., Tay, R.Y., Lukas, H., Sempionatto, J.R., Li, J., Xu, C., and Gao, W. (2024). A wearable aptamer nanobiosensor for non-invasive female hormone monitoring. Nat. Nanotechnol. *19*, 330–337. https://doi.org/10.1038/s41565-023-01513-0.
6. Zhao, J., Nyein, H.Y.Y., Hou, L., Lin, Y., Bariya, M., Ahn, C.H., Ji, W., Fan, Z., and Javey, A. (2021). A Wearable Nutrition Tracker. Adv. Mater. *33*, 2006444. https://doi.org/10.1002/adma.202006444.
7. Xu, C., Song, Y., Sempionatto, J.R., Solomon, S.A., Yu, Y., Nyein, H.Y.Y., Tay, R.Y., Li, J., Heng, W., Min, J., et al. (2024). A physicochemical-sensing electronic skin for stress response monitoring. Nat. Electron. *7*, 168–179. https://doi.org/10.1038/s41928-023-01116-6.
8. Xu, Y., De la Paz, E., Paul, A., Mahato, K., Sempionatto, J.R., Tostado, N., Lee, M., Hota, G., Lin, M., Uppal, A., et al. (2023). In-ear integrated sensor array for the continuous monitoring of brain activity and of lactate in sweat. Nat. Biomed. Eng. *7*, 1307–1320. https://doi.org/10.1038/s41551-023-01095-1.
9. Torrente-Rodríguez, R.M., Tu, J., Yang, Y., Min, J., Wang, M., Song, Y., Yu, Y., Xu, C., Ye, C., IsHak, W.W., and Gao, W. (2020). Investigation of cortisol dynamics in human sweat using a graphene-based wireless mHealth system. Matter *2*, 921–937. https://doi.org/10.1016/j.matt.2020.01.021.
10. Song, Y., Tay, R.Y., Li, J., Xu, C., Min, J., Shirzaei Sani, E., Kim, G., Heng, W., Kim, I., and Gao, W. (2023). 3D-printed epifluidic electronic skin for machine learning-powered multimodal health surveillance. Sci. Adv. *9*, eadi6492. https://doi.org/10.1126/sciadv.adi6492.
11. Choi, J., Ghaffari, R., Baker, L.B., and Rogers, J.A. (2018). Skin-interfaced systems for sweat collection and analytics. Sci. Adv. *4*, eaar3921. https://doi.org/10.1126/sciadv.aar3921.
12. He, W., Wang, C., Wang, H., Jian, M., Lu, W., Liang, X., Zhang, X., Yang, F., and Zhang, Y. (2019). Integrated textile sensor patch for real-time and multiplex sweat analysis. Sci. Adv. *5*, eaax0649. https://doi.org/10.1126/sciadv.aax0649.
13. Yin, L., Kim, K.N., Lv, J., Tehrani, F., Lin, M., Lin, Z., Moon, J.M., Ma, J., Yu, J., Xu, S., and Wang, J. (2021). A self-sustainable wearable multi-modular E-textile bioenergy microgrid system. Nat. Commun. *12*, 1542–1553. https://doi.org/10.1038/s41467-021-21701-7.
14. Bariya, M., Nyein, H.Y.Y., and Javey, A. (2018). Wearable sweat sensors. Nat. Electron. *1*, 160–171. https://doi.org/10.1038/s41928-018-0043-y.
15. Kim, D.H., Lu, N., Ma, R., Kim, Y.S., Kim, R.H., Wang, S., Wu, J., Won, S.M., Tao, H., Islam, A., et al. (2011). Epidermal electronics. Science *333*, 838–843. https://doi.org/10.1126/science.1206157.

16. Yang, Y., Song, Y., Bo, X., Min, J., Pak, O.S., Zhu, L., Wang, M., Tu, J., Kogan, A., Zhang, H., et al. (2020). A laser-engraved wearable sensor for sensitive detection of uric acid and tyrosine in sweat. Nat. Biotechnol. *38*, 217–224. https://doi.org/10.1038/s41587-019-0321-x.

17. Tu, J., Min, J., Song, Y., Xu, C., Li, J., Moore, J., Hanson, J., Hu, E., Parimon, T., Wang, T.Y., et al. (2023). A wireless patch for the monitoring of C-reactive protein in sweat. Nat. Biomed. Eng. *7*, 1293–1306. https://doi.org/10.1038/s41551-023-01059-5.

18. Gao, W., Emaminejad, S., Nyein, H.Y.Y., Challa, S., Chen, K., Peck, A., Fahad, H.M., Ota, H., Shiraki, H., Kiriya, D., et al. (2016). Fully integrated wearable sensor arrays for multiplexed in situ perspiration analysis. Nature *529*, 509–514. https://doi.org/10.1038/nature16521.

19. Wang, M., Yang, Y., Min, J., Song, Y., Tu, J., Mukasa, D., Ye, C., Xu, C., Heflin, N., McCune, J.S., et al. (2022). A wearable electrochemical biosensor for the monitoring of metabolites and nutrients. Nat. Biomed. Eng. *6*, 1225–1235. https://doi.org/10.1038/s41551-022-00916-z.

20. Ding, S., Saha, T., Yin, L., Liu, R., Khan, M.I., Chang, A.Y., Lee, H., Zhao, H., Liu, Y., Nazemi, A.S., et al. (2024). A fingertip-wearable microgrid system for autonomous energy management and metabolic monitoring. Nat. Electron. *7*, 788–799. https://doi.org/10.1038/s41928-024-01236-7.

21. Mahato, K., Saha, T., Ding, S., Sandhu, S.S., Chang, A.Y., and Wang, J. (2024). Hybrid multimodal wearable sensors for comprehensive healthy monitoring. Nat. Electron. *7*, 735–750. https://doi.org/10.1038/s41928-024-01247-4.

22. Gao, Y., Bi, L., Li, A., Du, M., Song, M., and Jiang, G. (2024). Associations of bisphenols exposure and hyperuricemia based on human investigation and animal experiments. Environ. Sci. Technol. *58*, 5290–5298. https://doi.org/10.1021/acs.est.4c00792.

23. Huang, Z., Xie, N., Illes, P., Di Virgilio, F., Ulrich, H., Semyanov, A., Verkhratsky, A., Sperlagh, B., Yu, S.G., Huang, C., and Tang, Y. (2021). From purines to purinergic signalling: molecular functions and human diseases. Signal. Transduct. Tar. *6*, 162. https://doi.org/10.1038/s41392-021-00553-z.

24. Stiburkova, B., Závada, J., Tomcik, M., Miyata, H., Toyoda, Y., Takada, T., and Suzuki, H. (2015). A2.5 Novel dysfunctional variant in ABCG2 gene is a cause of primary hyperuricemia and gout: biochemical, molecular genetic and functional analysis. Ann. Rheum. Dis. *74*, A17. https://doi.org/10.1136/annrheumdis-2015-207259.40.

25. Frohlich, E.D. (1993). Uric acid: A Risk Factor for Coronary Heart Disease. JAMA *270*, 378–379. https://doi.org/10.1001/jama.1993.03510030102044.

26. Yu, W., Xie, D., Yamamoto, T., Koyama, H., and Cheng, J. (2023). Mechanistic insights of soluble uric acid-induced insulin resistance: Insulin signaling and beyond. Rev. Endocr. Metab. Disord. *24*, 327–343. https://doi.org/10.1007/s11154-023-09787-4.

27. Roumeliotis, S., Roumeliotis, A., Dounousi, E., Eleftheriadis, T., and Liakopoulos, V. (2019). Dietary antioxidant supplements and uric acid in chronic kidney disease: a review. Nutrients *11*, 1911. https://doi.org/10.3390/nu11081911.

28. Stamp, L.K., Farquhar, H., Pisaniello, H.L., Vargas-Santos, A.B., Fisher, M., Mount, D.B., Choi, H.K., Terkeltaub, R., Hill, C.L., and Gaffo, A.L. (2021). Management of gout in chronic kidney disease: a G-CAN consensus statement on the research priorities. Nat. Rev. Rheumatol. *17*, 633–641. https://doi.org/10.1038/s41584-021-00657-4.

29. Nishikawa, K., Nagae, A., Miura, T., Fujimori, K., Sunohara, D., Yui, H., Maruyama, S., Nakamura, C., Tabata, H., Kashiwagi, D., et al. (2019). Impact of hyperuricemia on patients with diabetes mellitus who underwent percutaneous coronary intervention. J. Am. Coll. Cardiol. *73*, 115. https://doi.org/10.1016/s0735-1097(19)30723-5.

30. Lin, W.Y., Liu, C.S., Li, T.C., Lin, T., Chen, W., Chen, C.C., Li, C.I., and Lin, C.C. (2008). In addition to insulin resistance and obesity, hyperuricemia is strongly associated with metabolic syndrome using different definitions in Chinese populations: a population-based study (Taichung Community Health Study). Ann. Rheum. Dis. *67*, 432–433. https://doi.org/10.1136/ard.2007.073601.

31. Gao, B., Zhou, J., Ge, J., Zhang, Y., Chen, F., Lau, W.B., Wan, Y., Zhang, N., Xing, Y., Wang, L., et al. (2012). Association of maximum weight with hyperuricemia risk: a retrospective study of 21,414 Chinese people. PLoS One *7*, e51186. https://doi.org/10.1371/journal.pone.0051186.

32. Rubin, R.T., Rahe, R.H., Gunderson, E.K., and Clark, B.R. (1970). Motivation and serum uric acid levels. Percept. Mot. Skills *30*, 794. https://doi.org/10.2466/pms.1970.30.3.794.

33. Duan, W., Cheng, J., and Guo, J. (2022). Smartphone-based photochemical sensor for multiplex determination of glucose, uric acid, and total cholesterol in fingertip blood. Analyst *147*, 3285–3290. https://doi.org/10.1039/d2an00764a.

34. Nyein, H.Y.Y., Bariya, M., Tran, B., Ahn, C.H., Brown, B.J., Ji, W., Davis, N., and Javey, A. (2021). A wearable patch for continuous analysis of thermoregulatory sweat at rest. Nat. Commun. *12*, 1823. https://doi.org/10.1038/s41467-021-22109-z.

35. Gao, W., Ota, H., Kiriya, D., Takei, K., and Javey, A. (2019). Flexible electronics toward wearable sensing. Acc. Chem. Res. *52*, 523–533. https://doi.org/10.1021/acs.accounts.8b00500.

36. Brunmair, J., Gotsmy, M., Niederstaetter, L., Neuditschko, B., Bileck, A., Slany, A., Feuerstein, M.L., Langbauer, C., Janker, L., Zanghellini, J., et al. (2021). Finger sweat analysis enables short interval metabolic biomonitoring in humans. Nat. Commun. *12*, 5993. https://doi.org/10.1038/s41467-021-26245-4.

37. Rath, R.J., Herrington, J.O., Adeel, M., Güder, F., Dehghani, F., and Farajikhah, S. (2024). Ammonia detection: A pathway towards potential point-of-care diagnostics. Biosens. Bioelectron. *251*, 116100. https://doi.org/10.1016/j.bios.2024.116100.

38. Chen, X., Kim, D.H., and Lu, N. (2024). Introduction: wearable devices. Chem. Rev. *124*, 6145–6147. https://doi.org/10.1021/acs.chemrev.4c00271.

39. Nyein, H.Y.Y., Bariya, M., Kivimäki, L., Uusitalo, S., Liaw, T.S., Jansson, E., Ahn, C.H., Hangasky, J.A., Zhao, J., Lin, Y., et al. (2019). Regional and correlative sweat analysis using high-throughput microfluidic sensing patches toward decoding sweat. Sci. Adv. *5*, eaaw9906. https://doi.org/10.1126/sciadv.aaw9906.

40. Dryhurst, G. (1971). Primary products of electrochemical oxidation of uric acid in aqueous and methanolic solution. J. Electrochem. Soc. *118*, 699. https://doi.org/10.1149/1.2408147.

41. Alam, M.J., and Ahmad, S. (2015). FTIR, FT-Raman, UV-Visible spectra and quantum chemical calculations of allantoin molecule and its hydrogen bonded dimers. Spectrochim. Acta A. *136*, 961–978. https://doi.org/10.1016/j.saa.2014.09.119.

42. Singh, A., Sharma, A., and Arya, S. (2022). Deposition of Ni/RGO nanocomposite on conductive cotton fabric as non-enzymatic wearable electrode for electrochemical sensing of uric acid in sweat. Diam. Relat. Mater. *130*, 109518–109527. https://doi.org/10.1016/j.diamond.2022.109518.

43. Wang, C., Zhang, Y., Liu, Y., Zeng, X., Jin, C., Huo, D., Hou, J., and Hou, C. (2024). A wearable flexible electrochemical biosensor with CuNi-MOF@rGO modification for simultaneous detection of uric acid and dopamine in sweat. Anal. Chim. Acta *1299*, 342441. https://doi.org/10.1016/j.aca.2024.342441.

44. Zhang, B., Li, J., Zhou, J., Chow, L., Zhao, G., Huang, Y., Ma, Z., Zhang, Q., Yang, Y., Yiu, C.K., et al. (2024). A three-dimensional liquid diode for soft, integrated permeable electronics. Nature *628*, 84–92. https://doi.org/10.1038/s41586-024-07161-1.

45. Koratala, A., Singhania, G., Alquadan, K.F., Shimada, M., Johnson, R.J., and Ejaz, A.A. (2016). Serum uric acid exhibits inverse relationship with estimated glomerular filtration rate. Nephron *134*, 231–237. https://doi.org/10.1159/000448629.

46. Kan, Y., Zhang, Z., Yang, K., Ti, M., Ke, Y., Wu, L., Yang, J., and He, Y. (2019). Influence of d-amino acids in beer on formation of uric acid.

Food Technol. Biotechnol. *57*, 418–425. https://doi.org/10.17113/ftb.57.03.19.6022.

47. Alharbi, M.H., Alharbi, N.H.J., Brnawi, I.A., and Atiq, E.H. (2023). Implication of red meat consuption habits in serum uric acid levels and mood disorders among first-trimeter pregnant women. BMC Nutr. *9*, 111–118. https://doi.org/10.1186/s40795-023-00769-y.

48. Gibson, T., Rodgers, A.V., Simmonds, H.A., and Toseland, P. (1984). Beer drinking and its effect on uric acid. Br. J. Rheumatol. *23*, 203–209. https://doi.org/10.1093/rheumatology/23.3.203.

49. Trinchieri, A., and Montanari, E. (2017). Prevalence of renal uric acid stones in the adult. Urolithiasis *45*, 553–562. https://doi.org/10.1007/s00240-017-0962-5.